Incorporating Cs and Sr into blast furnace slag inorganic polymers and their effect on matrix properties

Incorporating Cs and Sr into blast furnace slag inorganic polymers and their effect on matrix properties

Niels Vandevenne [a], Remus Ion Iacobescu [b], Yiannis Pontikes [b], Robert Carleer [c], Elsy Thijssen [c], Katrijn Gijbels [a], Sonja Schreurs [a], Wouter Schroeyers [a,*]

[a] *Hasselt University, CMK, Nuclear Technological Centre (NuTeC), Faculty of Engineering Technology, Agoralaan, Gebouw H, 3590 Diepenbeek, Belgium*

[b] *KU Leuven, Department of Materials Engineering, Kasteelpark Arenberg 44, 3001 Leuven, Belgium*

[c] *Hasselt University, CMK, Research Group of Applied and Analytical Chemistry, Agoralaan, Gebouw D, 3590 Diepenbeek, Belgium*

* Corresponding author: Prof. dr. Wouter Schroeyers, e-mail address: wouter.schroeyers@uhasselt.be

Abstract

Minimizing harmful effects to the environment in waste-management practices requires continuous innovation. This is especially important in the field of radioactive waste management. Alternatives to the commonly used ordinary Portland cement matrices are being increasingly studied for improved immobilisation purposes. The development of inorganic polymers (IP) from industrial residues has been successfully studied for the immobilisation of caesium (Cs^+) and strontium (Sr^{2+}). However, knowledge of the effect of these introduced elements on the IP-matrix is scarce, especially considering that studied effects are dependent on the IP-precursor characteristics and the form in which the Cs^+ and Sr^{2+} are introduced. In this study, IPs containing varying amounts of $CsNO_3$ and $Sr(NO_3)_2$ were developed to study the effect of the introduced elements on the IP-characteristics. IP-samples were developed from ground granulated blast furnace slag (GGBFS) and 6 M NaOH activating solution. Cs^+ and Sr^{2+} were added to account for 0.5, 1 and 2 wt% of the total IP-mass. Throughout the entire study, Cs^+-addition showed no significant effects on the studied parameters. Calorimetric results showed that Sr^{2+} severely affects reaction kinetics, consuming hydroxide ions necessary for the alkali activation reaction. Sr^{2+}-addition also caused a severe decrease in compressive strength, increased calcium leaching, and decreased sodium and hydroxide leaching. Micro-chemical analyses showed that Cs^+ is almost fully incorporated in the formed IP-matrix, while Sr^{2+} mainly precipitates as $Sr(OH)_2$ in concentrated regions throughout the IP-structure. The findings presented in this paper give insights on the effect of contaminant elements on the immobilizing matrix.

Keywords

Inorganic polymer, waste immobilisation, slag, caesium, strontium, alkali activation

1 Introduction

To address health and environmental risks associated with long-term storage of radioactive waste (RAW), researchers have been looking for better performing alternatives to the ordinary Portland cement (OPC) matrices vastly used by the nuclear industry for RAW-immobilisation; these alternatives include calcium-sulfoaluminate-cement, calcium-aluminate-cement, and geopolymer/inorganic polymer-type matrices (based on metakaolin and sodium silicate) [1]. Immobilising hazardous cations like caesium-137 ($^{137}Cs^{+}$, $T_{1/2}$ = 30.05 a) and strontium-90 ($^{90}Sr^{2+}$, $T_{1/2}$ = 28.80 a) is key in handling RAW, especially concerning nuclear power plants [2,3], since these radionuclides are most often present in cooling water of nuclear reactors [4]. The main solidification mechanism for cationic species in OPC-based binders, which is based on precipitation of the corresponding hydroxides due to the highly alkaline pore solution, is not valid for Cs^{+} causing a low retention and high diffusion towards the biosphere [5]. According to Wieland et al. (2008), Sr^{2+}-uptake in OPC occurs mainly as partially hydrated species, binding Sr^{2+} to calcium-silicate-hydrate (C-S-H) phases [6]. They concluded that the Sr^{2+}-binding is mainly a reversible process, with only a small part of the Sr^{2+} being bound in the cement-structure, and that Sr^{2+} is bound to surface sites of C-S-H via bridging oxygen atoms through ion exchange interactions with Ca^{2+}, Na^{+} and K^{+} on silanol-groups of the C-S-H-phases (in line with an earlier study of Tits et al. (2006) [7]) [6].

A promising option for a more effective immobilisation matrix is the use of inorganic polymers (IPs). IPs generally demonstrate a higher fire/acid resistance in comparison to OPC and an increasing number of studies is dedicated to the suitability of IPs for RAW-immobilisation, using a variety of industrial wastes as precursors for the IPs [2,4,8–17]. However, introduced species can have a large impact on the properties of the immobilisation matrix, and this effect has been studied to a much lesser extent [18,19]. Also, the conclusions of these studies are not easily generalized due to high variability in precursor composition, and the differences between high-Ca and low-Ca precursors regarding the IP microstructure and strength development. Provis et al. (2008) studied the effect of

63 caesium and strontium salts (nitrates, sulphates and hydroxides) on metakaolin-based IPs and found
64 that insoluble $SrCO_3$ formed in all Sr^{2+}-containing samples [18]. They also found that the excess of
65 nitrates precipitates as $NaNO_3$ and that addition of $CsNO_3$ caused a clear delaying effect on
66 geopolymer binder formation, being significant even at 0.10 or 0.50 wt% $CsNO_3$. In addition, they
67 reported a disruption of the pore structure formation, caused by the presence of ions in the pore
68 solution (particularly the bulky NO_3^-); these anions are repelled by the negatively charged
69 aluminosilicate framework preventing condensation reactions from taking place [18]. This
70 obstruction of gel-hardening was also observed by Komnitsas et al. (2013), who found that the
71 compressive strength of their samples decreased by the presence of NO_3^- and SO_4^-, since these
72 consume part of the alkali activator cations, hindering the geopolymerization reactions [20]. Provis et
73 al. (2008) discussed that Sr^{2+} added as a nitrate will probably behave similarly to Ca^{2+} during
74 geopolymer formation [18]. They noticed a dramatic decrease in the resistivity of the geopolymer
75 binder and attributed this effect to the presence of the nitrate ion, causing a combination of
76 increased pore size and connectivity, and subsequent mobility of the nitrate ions through the
77 solution-filled pores [18]. They didn't observe this effect as strongly in the $CsNO_3$-containing samples
78 and attributed this to the lower nitrate concentration [18]. According to Kuenzel et al. (2015), Sr^{2+}
79 uptake in geopolymer activated by a Na^+-activating solution is limited to 0.4 mol Sr^{2+} per mol of
80 aluminium, and an excess of Sr^{2+} is immobilised by precipitation as hydroxide or carbonate phases
81 [4]. Peng et al. (2016) found that the addition of strontium to metakaolin-zeolite geopolymers caused
82 a hysteresis effect [19]. They attributed the longer setting time to three possible causes: (1)
83 precipitation of Sr^{2+} and OH^- or $[SiO_4]^{4-}$, passivating the surface of the precursors and slowing down
84 dissolution; (2) reaction of Sr^{2+} and OH^- or $[SiO_4]^{4-}$ resulting in a decrease in the number of hydroxide-
85 ions and silicon-oxygen tetrahedrons; (3) the introduced ions lower the diffusion rate of all ions
86 present in the system as a function of charge attraction and repulsion, and so postponing the
87 geopolymer gel formation [19]. They also reported that Sr^{2+} takes part in the polymerization reaction
88 and that the Sr^{2+}-ion can replace several Na^+-ions for charge balancing purposes [19].

Fewer studies exist on the use of alkali-activated ground granulated blast furnace slag (GGBFS) for immobilising caesium and strontium in comparison with e.g. alkali-activated metakaolin. According to Gong and White (2016),the primary reaction product in GGBFS-based IPs is a C-(N)-A-S-H gel (calcium-sodium-aluminium-silicate-hydrate), resembling a highly disordered C-S-H [21]. The reported use of IPs based on GGBFS for immobilising Cs^+ and Sr^{2+} is scarce [2,9]. Qian et al. (2001) prepared GGBFS IPs containing 0.5 wt% Cs^+ and Sr^{2+} and found them to immobilize Cs^+ and Sr^{2+} better than an OPC matrix [9]. A similar result was reported by Guangren et al. (2002) [2]. Some authors have added GGBFS as an additive in IPs based on different precursors [14,15,22]. However, the effect of caesium- and strontium-addition on the IP-characteristics is not thoroughly investigated. To fill this existing knowledge gap, IPs based solely on GGBFS and a NaOH activating solution are developed for the immobilisation of Cs^+ and Sr^{2+}. This paper discusses the effect of the introduced species on IP reaction kinetics and physical and mechanical properties.

2 Materials and methods

Commercially available GGBFS was used as a precursor for the IPs. The slag was first dried at 110 °C to constant weight and then milled for 6 h (Attritor ball mill type 1S, Wiener & Co.). The density of the slag was measured 2.91 ± 0.01 g/cm³ (Quantachrome Multipycnometer MVP-6DC). The fineness of the resulting GGBFS powder was measured according to EN 196-6 [23] and found to be 5900 ± 100 cm²/g. The chemical composition of the GGBFS was determined by means of X-ray fluorescence spectroscopy and is shown in **Table 1** (results expressed as oxide, except for Cl).

Table 1: GGBFS oxide and chloride composition.

Compound	wt%
CaO	42.4
SiO_2	33.5
Al_2O_3	11.3
MgO	8.5
SO_3	1.9
TiO_2	0.7

Na_2O	0.4
K_2O	0.4
Fe_2O_3	0.4
MnO	0.2
ZrO_2	0.1
SrO	0.1
Cl	0.1

109

110 IP-pastes were produced by mixing the prepared GGBFS-powder with a 6 mol/L NaOH activating
111 solution at a liquid-over-solid ratio (L/S) of 0.37, found to be the optimum in an earlier study [24].
112 The activating solution was prepared from NaOH-pellets (Fischer Scientific, 98.44 % pure) and type II
113 distilled water. Cs^+ and Sr^{2+} were added as nitrates ($CsNO_3$, Alfa Aesar 99.8%; $Sr(NO_3)_2$, Emsure
114 99.0%) to account for 0, 0.5, 1 and 2 wt% of the final IP-mass (solid precursor + activating solution +
115 added nitrates). These amounts were fixed based on literature and earlier experiments (among
116 which our earlier study [24]). The mixtures were cast in 20 x 20 x 80 mm^3 moulds and covered with
117 plastic foil to prevent dehydration. The hardened samples were demoulded after 1 day, placed in
118 plastic containers, and allowed to further cure at 21 ± 2 °C for a total curing time of 28 days. The mix
119 designs are given in Table 2.

120 **Table 2:** Inorganic polymer mix design (wt%).

	GGBFS	**NaOH (6 M)**	**Cs^+**	**Sr^{2+}**	**NO_3^-**
IP_0	72.96 ± 0.04	27.04 ± 0.04	-	-	-
IP_Cs_0.5	72.45 ± 0.01	26.81 ± 0.01	0.50 ± 0.01	-	0.23 ± 0.01
IP_Cs_1	71.92 ± 0.01	26.61 ± 0.01	1.00 ± 0.01	-	0.47 ± 0.01
IP_Cs_2	70.87 ± 0.02	26.21 ± 0.01	1.99 ± 0.01	-	0.93 ± 0.01
IP_Sr_0.5	72.12 ± 0.01	26.68 ± 0.01	-	0.49 ± 0.01	0.70 ± 0.01

IP_Sr_1	71.24 ± 0.01	26.36 ± 0.01	-	0.99 ± 0.01	1.41 ± 0.01
IP_Sr_2	69.48 ± 0.02	25.71 ± 0.01	-	1.99 ± 0.01	2.82 ± 0.01

All IPs were characterised for heat release and physical and mechanical properties. Additionally, morphological and micro-chemical analyses were performed at 28 days of curing. Leaching tests took place at 48 days of curing. To study the effect of Cs^{+} and Sr^{2+} addition on the heat released during the alkali activation process, a calorimetric study was performed under isothermal conditions (TAMIII Thermal Activity Monitor, TA Instruments). A weighed amount of dry precursor was placed in a vial, while a weighed amount of activating solution was brought into two syringes and placed on top of the vial. This combination was then inserted into the calorimeter. After a few hours, when the calorimeter obtained a steady background signal, the activating solution was injected into the vial, and mixed with the precursor. In this way, the heat release was monitored from the very start of the reaction.

To study morphology and micro-chemistry, a 28-day cured sample of each composition was cut with a low-speed diamond coated circular saw to 20 x 20 x 5 mm^3. This sample was then embedded in resin, polished, and carbon-coated. The micro-chemical analysis was performed with a Jeol Hyperprobe field emission gun electron probe micro-analyser (EPMA, JEOL JXA-8530F) equipped with five wavelength dispersive spectrometers (WDS). In addition to a point-based chemical analysis, the distribution of caesium and strontium was mapped for each of the samples. The EPMA was operated at 15 kV and a probe current of 15 nA. For quantitative elemental point analysis, the standards obsidian (for SiO_2, Na_2O, Al_2O_3), celestite (for SrO), and apatite (for CaO) were used, except for caesium, where a factory default standard was used instead, due to the unavailability of a known standard. Mappings for caesium were collected with a dwell time of 40 ms per pixel in an area of 750

x 575 pixels (pixel size 0.4 µm), and for strontium with a dwell time of 10 ms per pixel in an area of 1300 x 1000 pixels (pixel size 0.8 µm). The mapped surface area for caesium and strontium was 300 x 230 µm and 1040 x 800 µm, respectively.

The flexural (f_{cf}) and compressive strength (f_c) of the IP-pastes were measured at 1, 8 and 28 days. Of each composition, and at each time of sampling, three samples were used for the flexural strength. The sample dimensions were 20 x 20 x 80 mm³. For the compressive strength, six repetitions were performed using cubic samples of 20 x 20 x 20 mm³.

Determination of water absorption (E_v) (vacuum method), apparent porosity (P), apparent relative density (T), and bulk density (B) were performed following international standard ISO 10545-3 [25]. Results showed that the E_v and P were very low (< 1 %), and were not influenced by addition of strontium or caesium. T and B were both measured as 2.1 ± 0.1 g/cm³.

The capacity for immobilising Cs^+ and Sr^{2+}, and the release of the structural elements were determined by means of a dynamic diffusion test based on the standards ASTM C1220-98 [26] and EN/TS 15863:2015 [27]. IP-subsamples of 20 x 20 x 25 mm³ were cut from a larger 48-day-cured sample by means of dry cutting (to avoid premature wash-out). These samples were then cleaned using a dry brush, measured for dimensions and weight, and submerged in 400 ml of Milli-Q water while fixed in the centre of the water volume. Both container and sample holder were made of polypropylene. The containers were tightly closed and placed in an oven at 90 ± 2 °C for 7 days. At 1 h, 24 h, and 7 d after the start of the leaching experiment, the entire eluate volume was refreshed and aliquots were taken for further characterization. At each sampling time, 10.0 ml of the eluate was filtered over a 0.2 µm syringe filter and acidified immediately after sampling to a concentration of 1 % HNO_3 (MERCK Suprapur 65 %). The concentration of water-soluble Cs^+ was measured by ICP-MS (Perkin Elmer NexION 350S), while the concentrations of Sr^{2+}, Si^{4+}, Al^{3+}, Ca^{2+}, and Na^+ were measured by ICP-OES (Perkin Elmer type Optima 8300). The leaching experiment was performed in twofold for each of the IP-compositions. The results from the ICP-OES and ICP-MS measurements are

corrected for dilution and sample surface area. One blanc test per repetition was conducted simultaneously, using 400 ml of Milli-Q water in the exact same conditions, excluding the presence of a sample. The experimental results are expressed as the amount of the element released at sampling time (t), divided by the surface area of the sample (A). The cumulative release of each constituent can be calculated as:

$$R_i = \frac{\sum_0^n \left[\left(C_{i,n} - B_{i,n}\right) \cdot V\right]}{A} \quad (1)$$

With

R_i = cumulative release of element i (g/m²)

$C_{i,n}$ = concentration of element i in the filtered aliquot n (g/ml)

$B_{i,n}$ = concentration of element i in the filtered blanc aliquot n (g/ml)

V = initial volume of eluate in bottle containing sample matrix (ml)

A = surface of sample (m²)

Each sample was weighed before and after the leaching experiment. The loss of mass is similar for all samples (between 2 % and 6 %) and does not seem to be affected by the addition of caesium or strontium. At each sampling time, a portion of the eluate was used for measuring pH (calibrated electrode HI1043B, Hanna Instruments) and conductivity (Schott Geräte CG 858, calibrated with 0.1 M KCl), while another portion was used for titration purposes, to determine the amount of $^-$ hydrogen-consuming species released during the leaching process. Titration was performed in threefold using an automated burette (Metrohm Basic Titrino 794) with 0.1 M HCl. The HCl-solution was set with Na_2CO_3 dried at 110 °C as the primary standard.

3 Results and discussion

Figure 1 shows a visual difference between strontium- and caesium-containing samples. The photographs are taken after 8 days of curing. The white spots observed in the strontium-containing samples are most likely crystals of $Sr(OH)_2$ (see later section 3.1).

Figure 1. Visual difference between samples containing strontium or caesium. Samples from left to right: IP_0, IP_Cs_0.5, IP_Cs_1, IP_Cs_2, IP_Sr_0.5, IP_Sr_1, IP_Sr_2.

3.1 Calorimetry

The isothermal calorimetry results are given in **Figure 2**, showing the evolution of the heat released during the alkali activation process of the GGBFS-precursor, and the effect of caesium and strontium additions. The first stage of the reaction is a very fast and exothermic process, reaching a maximum heat flow of about 32 J h^{-1} g^{-1} (per gram of solid precursor) for IP_0. This maximum is reached about 50 min after adding the activating solution. The initial heat release is due to sorption of the activating solution on the precursor surface (weathering) and the dissolution of the solid aluminosilicate. After this, a lower but continuous heat release is measured due to ongoing polymerisation reactions [28]. The results from **Figure 2** indicate that addition of Cs^{+} has little to no effect on the heat released during the alkali activation process. Only a small variation in the maximum heat flow can be observed (peak measurement of 32.2 J h^{-1} g^{-1} for IP_0 and 29.9 J h^{-1} g^{-1} for IP_Cs_2), while no time delay of the maximum takes place. Addition of Sr^{2+}, however, does show a clear effect on the heat flow during the activation process. When increasing the amount of Sr^{2+}, an increasingly distinct peak appears before the initial weathering takes place (e.g. the peak of 25.36 J h^{-1} g^{-1} for IP_Sr_1). This initial peak can be attributed to the formation of $Sr(OH)_2$ immediately after adding the activating solution to the dry precursor (with $Sr(NO_3)_2$ mixed in). This reaction consumes a portion of the hydroxide ions, preventing them to participate in the alkali activation process. This effect would be manifested in a lower heat flow and a horizontal shift (time delay) of the peak (e.g. 21.34 J h^{-1} g^{-1} for IP_Sr_1) to the right. These slower dissolution kinetics are in line with the observed effect of strontium on the setting time of GGBFS IPs reported in an earlier study [24], where it was found that the setting time of a GGBFS-IP-paste is severely delayed by addition of Sr^{2+}. The less profound activation reaction for

IP_Sr_1 and IP_Sr_2 (measured as lower heat release, **Figure 2**) also leads to a decreased compressive strength (see section 3.3, **Figure 5**). During the mixing and casting procedure of the IP-samples, the addition of strontium also led to a more viscous mixture.

It is assumed that strontium hydroxide is formed immediately when Sr^{2+} comes into contact with the activating solution. Equation (2) assumes that the sodium- and nitrate-ions remain dissociated, while equation (3) assumes that the sodium and nitrate will precipitate to form $NaNO_3$. The crystallization of $NaNO_3$ from the pore solution has been reported by Provis et al. (2008) [18] and Blackford et al. (2007) [12] (both metakaolin-based IPs) when adding $Sr(NO_3)_2$, although not immediately during mixing, in contrast to the $Sr(OH)_2$ formation.

$$Sr(NO_3)_2 + 2\ Na^+ + 2\ OH^- \Rightarrow Sr(OH)_2 + 2\ Na^+ + 2\ NO_3^- \quad (2)$$

$$Sr(NO_3)_2 + 2\ Na^+ + 2\ OH^- \Rightarrow Sr(OH)_2 + 2\ NaNO_3 \quad (3)$$

Since the formation of $NaNO_3$ has been reported to take place during a later drying stage [18], it would thus not cause an immediate energy release during initial mixing. In **Figure 2**, however, for sample IP_Cs_2 a small “shoulder” in the curve is observed; since the amount of nitrates present in this sample is quite high, this could be due to formation of $NaNO_3$ or the prevention of condensation reactions by the NO_3^- ions as reported by [18,20]. The consumption of hydroxide ions by the introduced strontium reduces the amount available for the activation reaction, which is also reflected in the decreased OH^--leaching in the strontium-containing samples (later section 3.4.4, **Figure 12**). The white spots observed in the strontium-containing samples (see **Figure 1**) are most likely regions of $Sr(OH)_2$, which precipitate as a fine white crystalline solid.

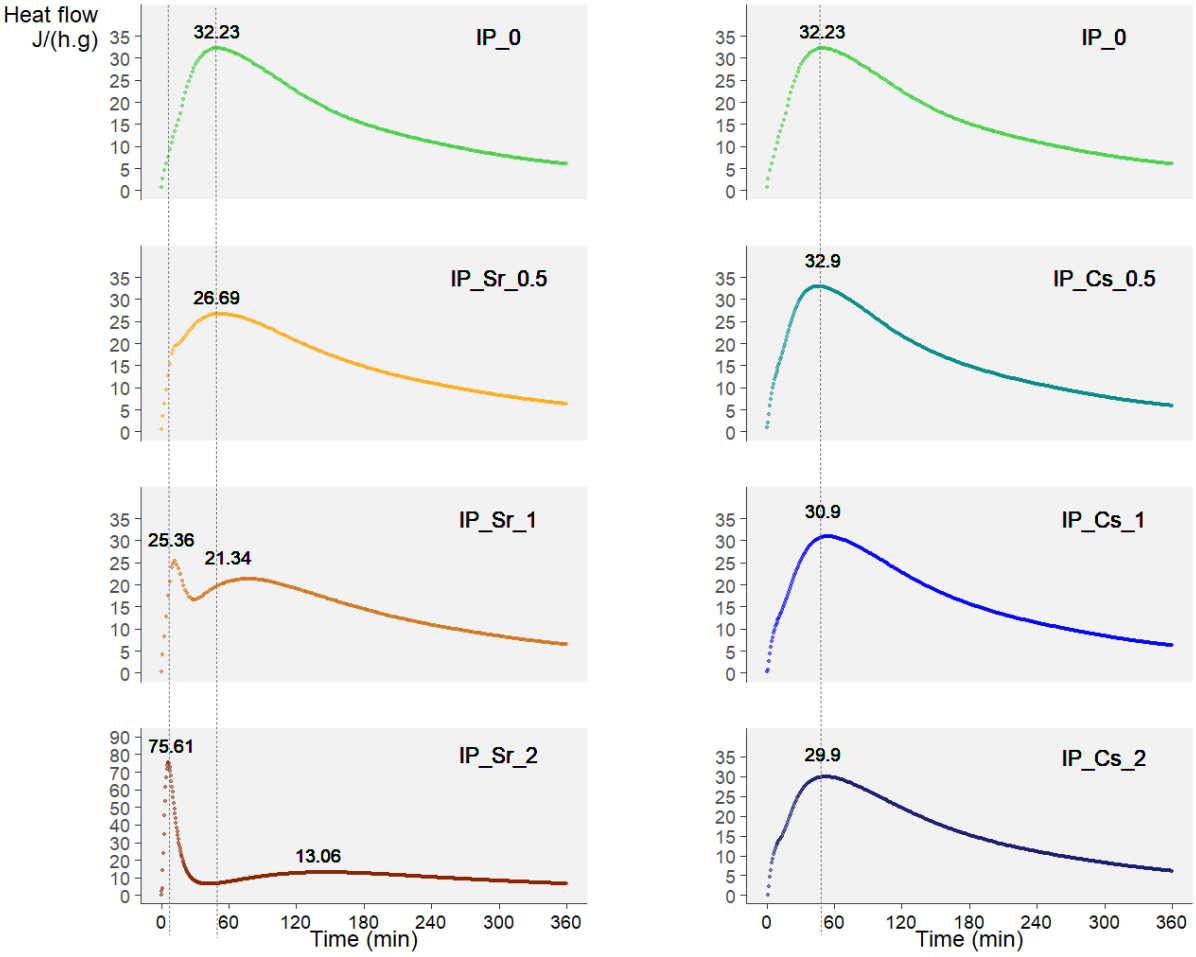

235

236 **Figure 2:** Effect of adding Sr^{2+} and Cs^{+} on the heat released per gram of solid precursor (J h^{-1} g^{-1})

237 during alkali activation of GGBFS.

238 *3.2 Micro-chemical analysis*

239 The results from the WDS micro-chemical analyses on the IP-samples are shown in **Table 3**. It is

240 important to note that the amounts given in **Table 3** are weight-percentages of the IP-matrix formed

241 by the activation process, excluding the undissolved precursor particles (hereafter referred to as

242 *matrix*), and not of the total IP-mass (hereafter referred to as IP_m). The fractions of introduced

243 strontium and caesium that are incorporated into the matrix, taking into account the ratio of formed

244 matrix over undissolved precursor, are determined by the following approach: using *Particle (Pores)*

245 *and Cracks Analysis System (PCAS)* software, a number of images were separately analysed to

246 average the surface ratios of matrix over undissolved precursor, which was found to be about 65/35.

Since this ratio is obtained using different images of randomly cut samples, it can also be assumed valid as a volume over volume ratio. Using this ratio, the density of the matrix phase is found to be 1.7 g/cm³, calculated using equation (4). The matrix phase, and the calculated density include possible pores and cracks. But since the open porosity is very low (see section 2), this influence is expected to be limited. The measured amounts of caesium and strontium (**Table 3**) in the matrix are converted to their respective fractions in the total IP-sample using equation (5).

$$\rho_M = \frac{\rho_{IP_m} - 0.35 * \rho_{GGBFS}}{0.65} \quad (4)$$

$$wt\%_{IP_m} = \frac{wt\%_M * 0.65 * \rho_M}{\rho_{IP_m}} \quad (5)$$

With

ρ_M = density of the matrix (g/cm³)

ρ_{IP_m} = density of the total inorganic polymer sample (2.1 g/cm³, see section 2)

ρ_{GGBFS} = density of the GGBFS precursor (2.91 g/cm³, see section 2)

$wt\%_{IP_m}$ = weight-percentage of Cs^+ or Sr^{2+} in the total inorganic polymer sample

$wt\%_M$ = weight-percentage of Cs^+ or Sr^{2+} in the matrix phase (as tabulated in **Table 3**)

For each measured $wt\%_M$, the calculated $wt\%_{IP_m}$ is given in **Table 4**, together with the fractions of the introduced caesium and strontium that are incorporated in the matrix ($wt\%_{IP_m}$ divided by 0.5, 1 or 2 wt%, multiplied by 100 %). Because of the uncertainty in the 65/35 ratio, the values in **Table 4** are given as estimates. From these values it can be deduced that for caesium, about all of the introduced Cs^+ is incorporated into the IP-matrix. These findings are in line with the study of Blackford et al. (2007), who reported that Cs^+ is fully incorporated at the nm-scale into the amorphous geopolymer phase [12]. For Sr^{2+}, the amounts shown in **Table 4** are corrected for the initial strontium-content measured in IP_0; the tabulated wt% are thus the amounts of Sr^{2+}

incorporated in the IP-matrix in addition to the inherent strontium from the precursor. From these results it can be concluded that in every step of strontium addition (0.5, 1, and 2 wt%), about one sixth is incorporated into the IP-matrix. Results from **Table 3** indicate that addition of strontium or caesium has no effect on the amounts of silicon, aluminium and sodium in the matrix. However, a small effect on the amount of calcium is observed. Adding caesium seems to cause a slight decrease of the Ca^{2+}-content, possibly caused by Cs^{+} replacing Ca^{2+}, since Ca^{2+} can act as a charge balancing ion [29].

Table 3: Results of micro-chemical analysis using EPMA (calculated from oxides).

Element (wt%)	**IP_0**	**IP_Sr_0.5**	**IP_Sr_1**	**IP_Sr_2**
Si^{4+}	13 ± 1	13 ± 1	12.6 ± 0.6	13 ± 1
Al^{3+}	5.3 ± 0.3	6 ± 1	5.5 ± 0.3	6.1 ± 0.6
Ca^{2+}	16.2 ± 0.9	17 ± 2	17 ± 1	17 ± 2
Na^{+}	2.0 ± 0.6	1.9 ± 0.5	2.6 ± 0.7	2.5 ± 0.4
Sr^{2+}	0.20 ± 0.02	0.36 ± 0.01	0.47 ± 0.09	0.9 ± 0.1
Cs^{+}	-	-	-	-
Element (wt%)		**IP_Cs_0.5**	**IP_Cs_1**	**IP_Cs_2**
Si^{4+}		13 ± 1	13 ± 1	12.5 ± 0.9
Al^{3+}		6.2 ± 0.6	5.8 ± 0.7	5.7 ± 0.8
Ca^{2+}		12 ± 2	13 ± 1	12.8 ± 0.7
Na^{+}		3.6 ± 0.4	2.5 ± 0.8	2.9 ± 0.4
Sr^{2+}		0.19 ± 0.02	0.19 ± 0.03	0.19 ± 0.02
Cs^{+}		1.32 ± 0.09	1.8 ± 0.4	3.6 ± 0.4

Table 4. (a) Weight-percentages of caesium and strontium incorporated in the matrix phase, recalculated for the entire IP-mass, and corrected for initial strontium content. (b) Percentages of introduced caesium and strontium that are incorporated into the matrix.

(a) $wt\%_{IP_{M,cor}}$	**IP_Sr_0.5**	**IP_Sr_1**	**IP_Sr_2**	**IP_Cs_0.5**	**IP_Cs_1**	**IP_Cs_2**
Sr^{2+}	0.08	0.14	0.36	-	-	-
Cs^{+}	-	-	-	0.68	0.93	1.86
(b) Fraction incorporated into matrix (%)						
Sr^{2+}	17	14	18	-	-	-
Cs^{+}	-	-	-	100*	93	93

* This value is rounded down since the calculated value is 137 % (probably due to statistical variation in the concentrations at the measurement points)

Figure 3 and **Figure 4** show mappings of these same samples to study the distribution of caesium and strontium throughout the microstructure. Mapping of the Sr^{2+}-containing samples is done at a larger scale than for the Cs^{+}-samples because this allows a clear view of precipitation sites for $Sr(OH)_2$, while the smaller scale for the Cs-samples allows a clearer view of the incorporation of Cs^{+} in the binder. For the samples containing added strontium, precipitation sites are clearly visible where large amounts of strontium are concentrated. From **Figure 3**, sample IP_Sr_0.5, it can be observed that a small amount of strontium is distributed evenly throughout the microstructure. **Figure 3** also shows large pores where the Sr^{2+} seems to be concentrated. **Figure 4** shows that Cs^{+} is incorporated homogeneously throughout the binder-phase. This difference in incorporation is also reflected in the leaching results (see further, section 3.4), where Cs^{+} leaches out more easily since it is distributed evenly throughout the structure (and thus being more available at the sample surface), while Sr^{2+} is more physically encapsulated (and thus less available at the sample surface).

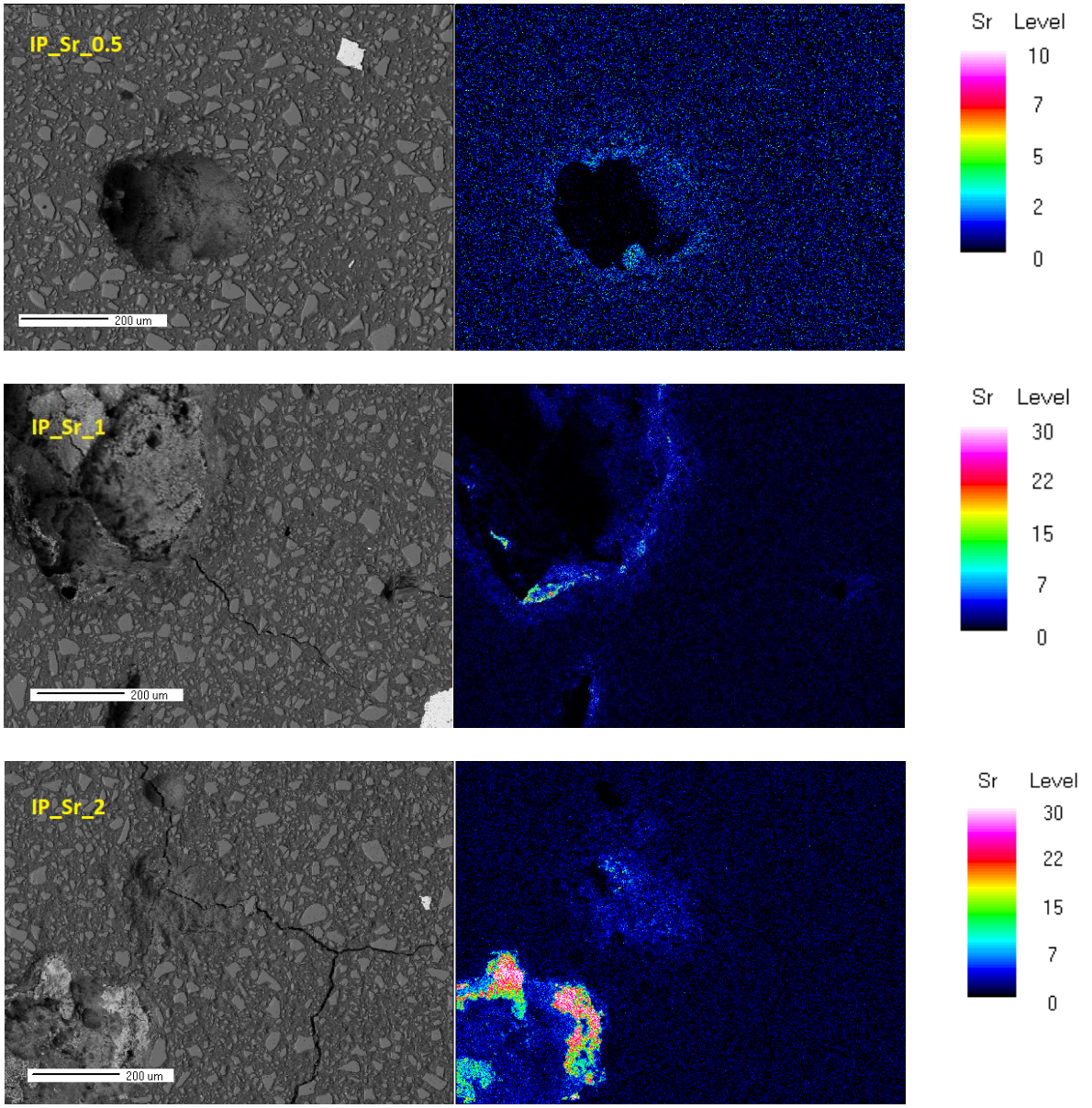

296 **Figure 3:** EPMA mappings of IP_Sr_0.5, IP_Sr_1 and IP_Sr_2. The level-scale of IP_Sr_0.5 is smaller for
297 improved visibility of the distribution of strontium throughout the matrix. The chemical composition
298 of the samples is given in **Table 3**.

299

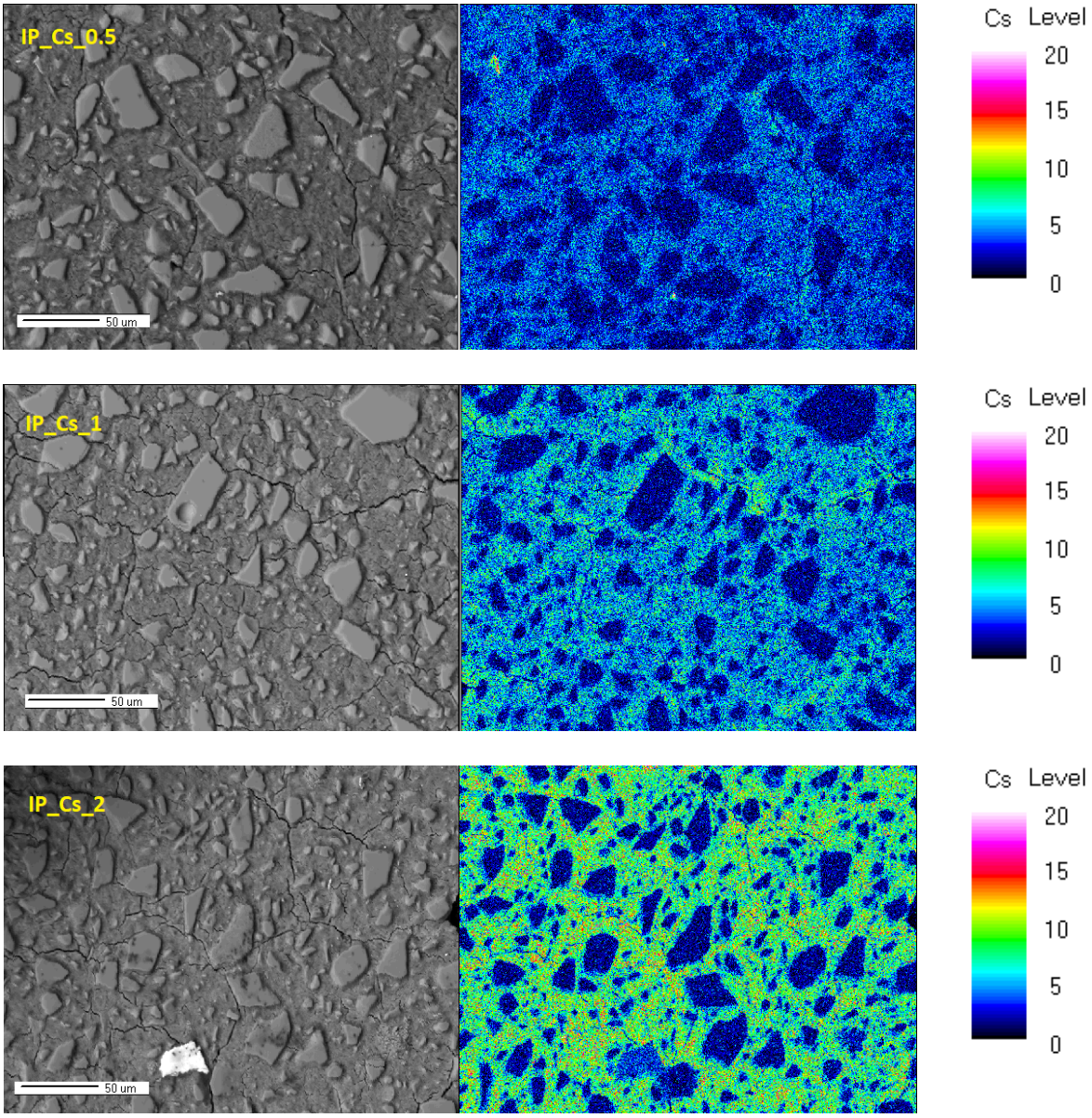

Figure 4: EPMA mappings of IP_Cs_0.5, IP_Cs_1 and IP_Cs_2. The chemical composition of the samples is given in **Table 3**.

3.3 Compressive and flexural strength

The compressive strength data shown in **Figure 5** indicate that addition of $CsNO_3$ does not significantly affect the strength development. Addition of $Sr(NO_3)_2$, however, does show a deleterious effect on the compressive strength. After 1 day and 8 days of curing, the compressive strength of IP_Sr_2 is only about 45 % of the values for IP_0. This difference is reduced with increased curing time. At 28 days of curing, IP_Sr_2 (19 ± 5 MPa) reaches about 60 % of the

compressive strength of IP_0 (31 ± 7 MPa). This negative effect on the compressive strength is probably caused by the less profound alkali activation reaction due to the formation of $Sr(OH)_2$ and $NaNO_3$, causing a less concentrated activating solution and resulting in slower dissolution kinetics (as discussed in section 3.1, and observed in an earlier study [24] as a longer setting time). The occurrence of $Sr(OH)_2$ precipitation spots and accompanying pores (see **Figure 1** and **Figure 3**) can also cause weak spots in the IP-structure. Provis et al. (2008) found that, in a metakaolin-based system, the addition of $CsNO_3$ caused a clear delaying effect on geopolymer gel formation, being significant even at 0.10 or 0.50 wt% $CsNO_3$, and attributed this to the presence of NO_3^- [18]. Since no negative effect is observed in the caesium-containing samples in this study, the decrease in compressive strength for the strontium-containing samples cannot be attributed to the presence of nitrates, but rather the presence of Sr^{2+}. A similar conclusion can also be drawn from an earlier study [24] where it was found that adding up to 2 wt% Cs^+ (in the form of nitrates) only showed a small effect on the final setting time (delay of up to 40 %), while strontium-addition retarded final setting severely (delay of 140 % at 0.5 wt% Sr^{2+}). For the flexural strength of the samples, the standard deviations are much too high to distinguish clearly between the results. Only at 1 day and 8 days of curing, there is a small discernible difference between IP_0 (1d: 9 ± 1 MPa; 8d: 12 ± 1) and IP_Sr_2 (1d: 7 ± 1 MPa; 8d: 9 ± 2 MPa). At 28 days of curing, no significant difference was observed.

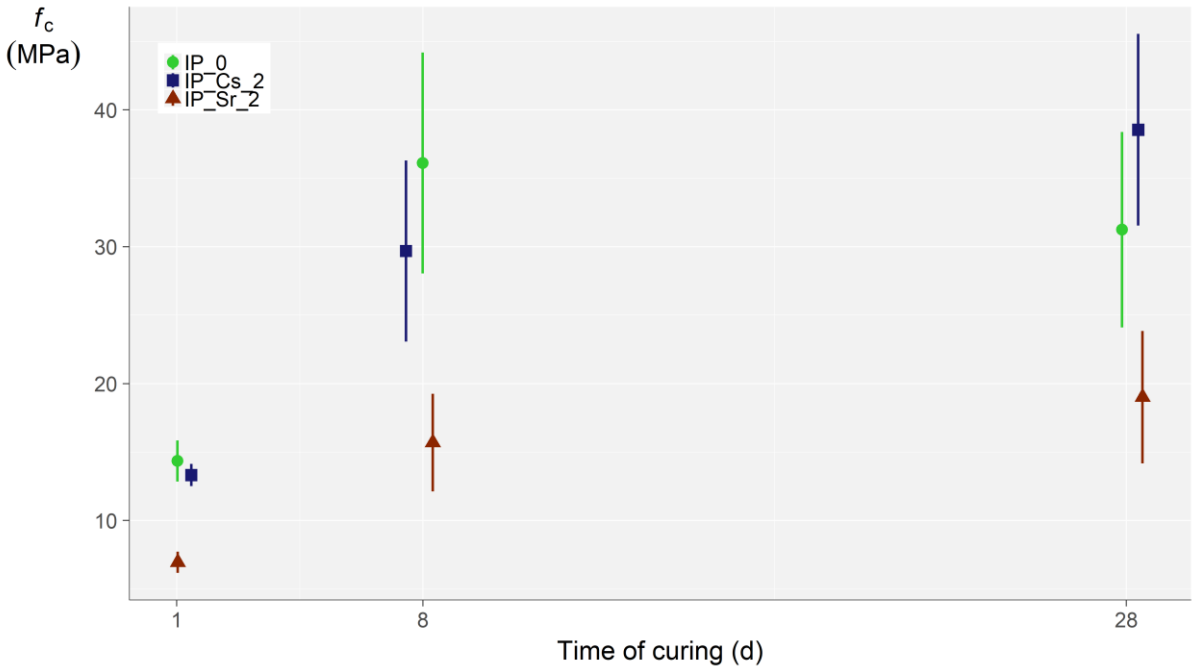

Figure 5: Compressive strength of IP_0, IP_Sr_2 and IP_Cs_2. Measurement points have been randomly offset from the times of curing (1 d, 8 d, and 28 d) for increased discernibility.

3.4 Leaching of structural and added elements

By use of a dynamic accelerated leaching test, the amount of Cs^+, Sr^{2+}, and structural elements released has been studied. For the release of caesium and strontium, only results are shown from the samples where the respective elements were added, together with IP_0. Overall, the measurement points lie very close together.

3.4.1 Release of Cs^+

The results of IP_Cs_0.5, IP_Cs_1 and IP_Cs_2 (**Figure 6**) show that the amount of Cs^+ released increases proportionally with the amount of Cs^+ introduced in the IP-matrix. There is no obvious change in leaching behaviour when adding more Cs^+, only an increase in the total amount released. When taking into account the amount of Cs^+ introduced into each sample, the mass of the sample, and the total amount of Cs^+ leached out, the percentage of introduced Cs^+ that was released can be determined. For IP_Cs_0.5, IP_Cs_1, and IP_Cs_2 this is respectively 63 %, 66 %, and 62 %. This

finding is in line with the proportional caesium-incorporation in the IP-binder, discussed in paragraph 3.2.

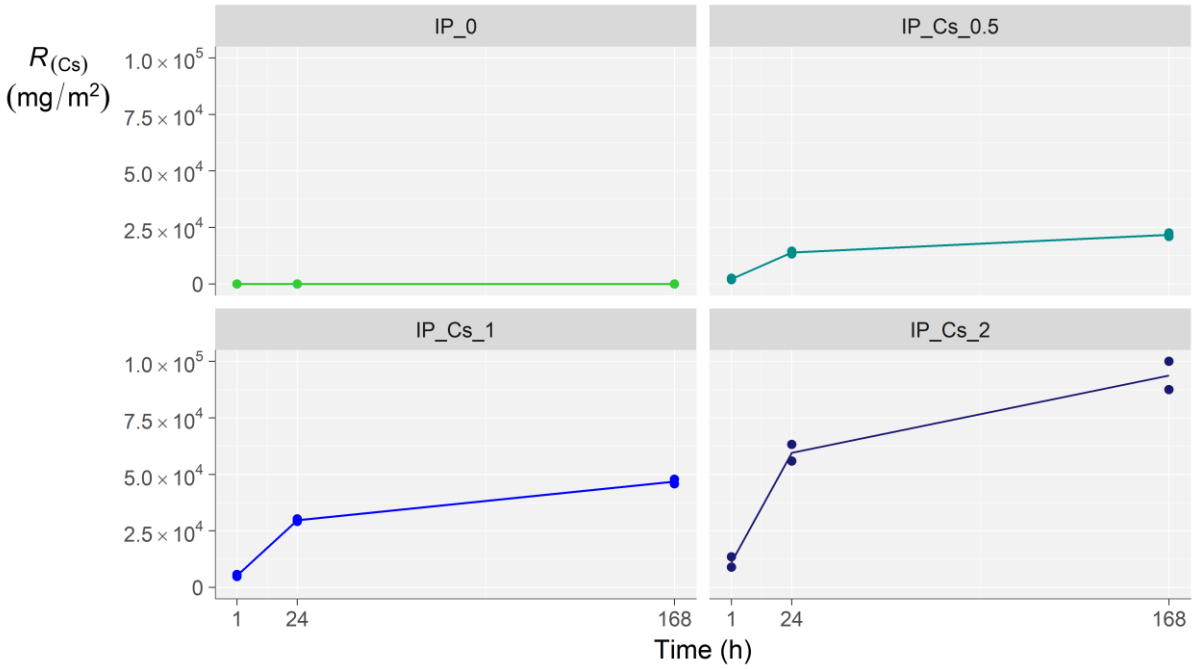

Figure 6: Cumulative release of Cs^{+} during a 7-day dynamic leaching test.

3.4.2 Release of Sr^{2+}

A small amount of Sr^{2+}, present in the GGBFS, leaches out from the base sample IP_0 (about 35 mg/m² after 7 days). When adding increasing amounts of Sr^{2+}, a proportional increase in Sr^{2+}-release is not immediately observed (see **Figure 7**). The measurement results are also less precise than the results for the other elements. This is most likely due to the fact that a large part of the Sr^{2+} is precipitated in the IP-structure as $Sr(OH)_2$ (as discussed in sections 3.1 and 3.2). This causes a distribution of precipitation sites (see **Figure 1**). Due to the casting process and cutting of the samples into smaller subsamples, a variation occurs in the amount of precipitated $Sr(OH)_2$ spots on or near the surface of the samples. This causes a variation in the amount of $Sr(OH)_2$ available for immediate dissolution from these precipitation spots. The amounts of introduced Sr^{2+} that were released, are 3 %, 2 %, and 4 % for IP_Sr_0.5, IP_Sr_1, and IP_Sr_2 respectively.

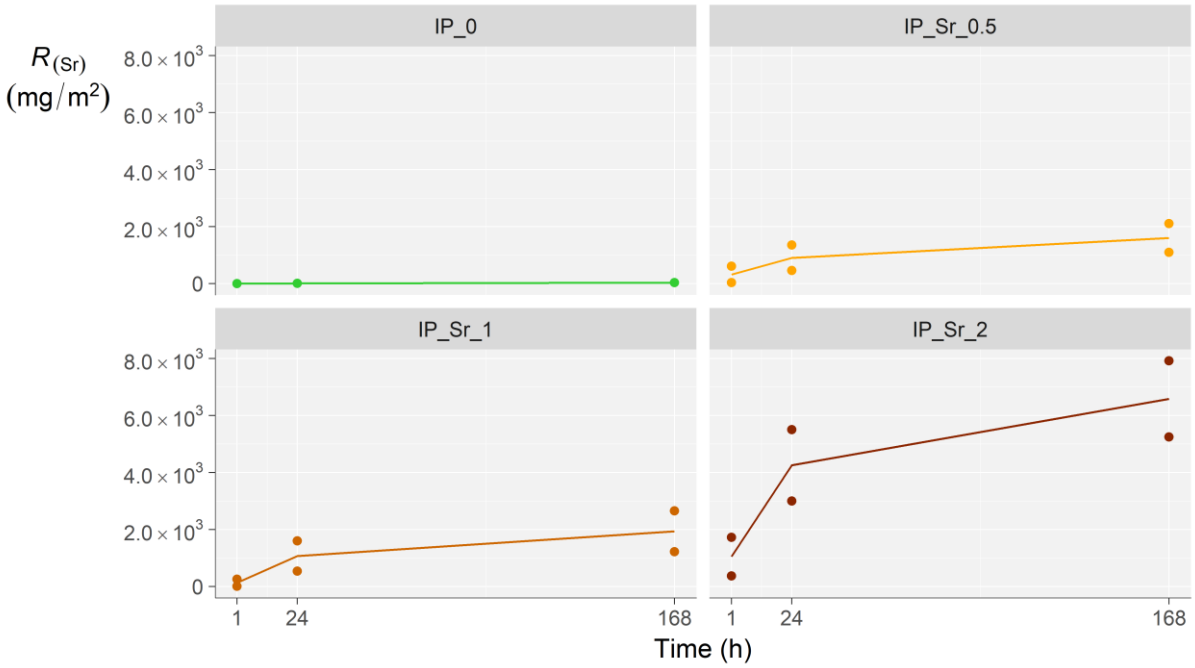

355

356 **Figure 7:** Cumulative release of Sr^{2+} during a 7-day dynamic leaching test.

357 *3.4.3 Release of structural elements*

358 **Figure 8** and **Figure 9** show the cumulative release of Al^{3+}, Si^{4+}, Ca^{2+} and Na^{+} respectively. Al^{3+}-release
359 of about 2000 mg/m² for IP_0, IP_Cs_0.5, IP_Cs_1 and IP_Cs_2 is observed. Addition of Cs^{+} to the
360 base IP does not seem to affect the leaching of Al^{3+} from the IP-matrix. Addition of Sr^{2+}, however,
361 does show a decrease in the amount of Al^{3+} released during leaching, dropping to a value of about
362 1400 mg/m² for IP_Sr_2. The reason for this is unclear. **Figure 8** shows cumulative Si^{4+}-release of
363 about 1750 mg/m² for all samples. Addition of Cs^{+} or Sr^{2+} does not seem to have any effect on the
364 amount of Si^{4+} released. Cumulative Ca^{2+}-release of about 5000 mg/m² is reached for IP_0, IP_Cs_0.5,
365 IP_Cs_1 and IP_Cs_2. Addition of Cs^{+} to the base IP does not seem to affect the leaching of Ca^{2+} from
366 the IP-matrix. Addition of Sr^{2+}, however, does show a slight increase in the amount of Ca^{2+} released
367 during leaching, rising to a value of about 6500 mg/m². A possible explanation for this is that the
368 added Sr^{2+} can replace Ca^{2+} as a charge-balancing ion, since Sr^{2+} can behave similarly to Ca^{2+} during IP
369 formation [18]. Also, since high-calcium GGBFS precursors give rise to calcium-(aluminium)-silicate-
370 hydrate (C-(A)-S-H) formation [21], it could be that Sr^{2+} replaces Ca^{2+} in the C-S-H, giving rise to a C-
371 (Sr)-A-S-H phase. This is in line with the findings of Wieland et al. (2008) and Tits et al. (2006), where

372 strontium-uptake in cementitious materials occurred through ion exchange with Ca^{2+} on silanol-
373 groups of the C-S-H-phases [6,7]. Both options would result in a structure where Ca^{2+} is less strongly
374 bound in the microstructure. This can also be seen in section 3.2, **Table 3** where the amount of Ca^{2+}
375 measured in the IP-matrix decreases slightly when adding more Sr^{2+}. **Figure 9** shows cumulative Na^{+}-
376 release of about 1.5 x 10^5 mg/m² for IP_0 and IP_Cs_2. Addition of Sr^{2+} seems to cause a significant
377 decrease in the amount of Na^{+} released during leaching, dropping to a value of about 7.5 x 10^4
378 mg/m² for IP_Sr_2, which is half of the Na^{+}-release from IP_0. This could be caused by the formation
379 of $NaNO_3$ as discussed in section 3.1, and further elaborated in the next section (3.4.4). The
380 formation of $NaNO_3$ seems to be a plausible cause, since Kuenzel et al. (2015) observed an increase
381 in Na^{+}-leaching when adding strontium in the form of $Sr(OH)_2$ to their IP-mixture (and thus having no
382 nitrates in their samples) [4]. Since the EPMA measurements (see section 3.2, **Table 3**) do not
383 indicate a difference in Na^{+} content in the IP-matrix, it can be deduced that the formation of $NaNO_3$
384 occurs after 28 days (EPMA was performed on 28-day-cured samples, while leaching was performed
385 on 48-day-cured samples). Since the samples for the leaching test were cut and transported in
386 ambient conditions, it is also likely that some drying occurred, increasing the formation of $NaNO_3$ (as
387 mentioned by Provis et al. (2008) that $NaNO_3$ crystallization from the pore solution could occur
388 during drying of the sample [18]). Addition of Cs^{+} to the base IP does not seem to affect the leaching
389 of Na^{+} from the IP-matrix. This indicates that adding $CsNO_3$ does not cause the formation of $NaNO_3$.
390 The latter was also reported by Blackford et al. (2007), who observed no formation of $NaNO_3$ when
391 adding $CsNO_3$, while $Sr(NO_3)_2$ addition did cause $NaNO_3$ crystallization [12].

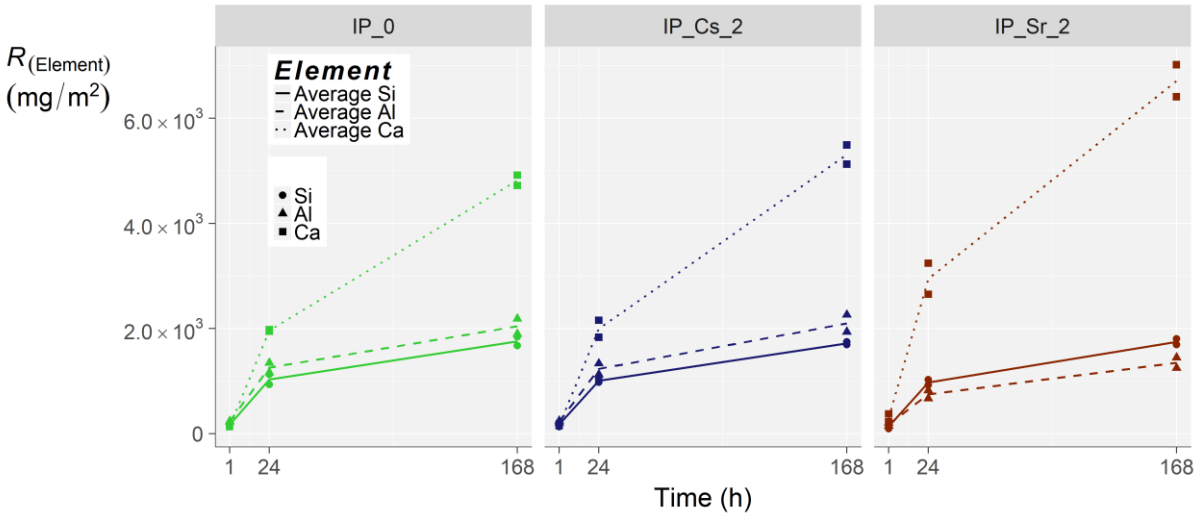

Figure 8: Cumulative release of Si^{4+}, Al^{3+}, and Ca^{2+} during a 7-day dynamic leaching test.

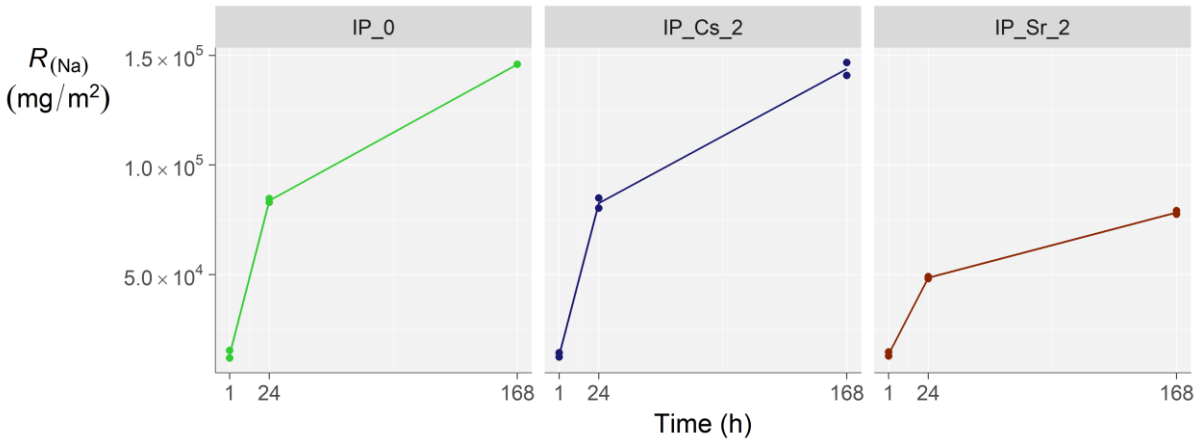

Figure 9: Cumulative release of Na^{+} during a 7-day dynamic leaching test.

3.4.4 Characterizing eluate

Figure 10 shows the measured pH-values of the eluate at different sampling times (1 h, 24 h, and 168 h after start leaching). These results show that the addition of caesium to the base IP-mixture does not have a significant effect on the pH of the eluate. Adding strontium, however, does show an influence on the pH of the eluate, decreasing gradually with increasing amounts of strontium (from pH 11.9 for IP_0 to pH 11.6 for IP_Sr_2). This decrease in pH is to be expected when $Sr(OH)_2$ is formed, trapping part of the introduced hydroxides in the IP-structure, and thus preventing them from leaching out. Regarding the conductivity of the eluate (**Figure 11**), the addition of caesium to

the base IP-mixture again doesn't show any significant change, while a clear change is observed when adding strontium. When adding 2 wt% of strontium to the base IP-mixture, a drop to about half is observed in the conductivity of the eluate (at 24 h and 168 h after the start of the leaching test). Taking into account the measured ions in the eluate (section 3.4), this change in conductivity seems most likely to be the cause of the lower Na^+-leaching in the strontium-containing samples. However, since the conductivity is also influenced by other charged species, the amount of hydrogen-consuming ions released in the eluate is also determined by use of automatic titration.

Figure 12 shows the results of the titration tests. During titration, 3 equivalence points were measured (around pH 10, pH 8.5, and pH 5). The positions of these equivalence points did not depend on the sampling time of the leaching test (1 h, 24 h, 168 h). The presence of these three equivalence points indicates that other hydrogen-consuming species (besides hydroxides) are present in the eluate. When comparing the results in **Figure 12** from the base IP-mixture (IP_0) and the caesium containing samples (IP_Cs_0.5, IP_Cs_1, and IP_Cs_2), no clear difference is observed in the amount of H^+-ions necessary to reach equivalence, and thus in the release of hydrogen-consuming species during leaching. The results from the strontium-containing samples (IP_Sr_0.5, IP_Sr_1, and IP_Sr_2), however, do show an effect on the amount of H^+-ions necessary for equivalence. After 1 h of leaching a small difference is already visible for IP_Sr_1 and IP_Sr_2. At the 24 h and 168 h sampling times, this difference has increased, indicating that the eluate from e.g. IP_Sr_2 contains about half the amount of hydrogen-consuming species compared to the eluate of IP_0. The number of hydroxide-ions released, calculated from the measured pH-values, is 37 ± 2 % of the amount of total hydrogen-consuming species (see **Figure 12**) for all samples over the total leaching period, leaving about 60 % for other unidentified hydrogen-consuming species.

Calculated from the measured pH-values, the eluates of IP_Sr_0.5, IP_Sr_1 and IP_Sr_2 contain respectively about 17 %, 40 % and 50 % less hydroxide-ions then the eluate of IP_0. The trend observed when adding increasing amounts of strontium to the base mixture is similar for the

measured Na^+-concentration, conductivity, and OH^--concentration. Results for all three parameters seem to drop slightly when adding 0.5 wt% strontium, while dropping by about 35-40 % and 50 % when adding 1 and 2 wt% respectively. From this, it can be concluded that the amounts of OH^- and Na^+ released during leaching are closely linked, and affected similarly when adding strontium. A first possible explanation for the lower release of both OH^- and Na^+ when adding increasing amounts of strontium can be that strontium hydroxide is formed immediately when Sr^{2+} comes into contact with the activating solution (see section 3.1). Since the positive Sr^{2+}-ions are consumed by the hydroxide-ions, the remaining NO_3^--anions could cause the Na^+-cations to be more strongly retained due to ionic interaction or $NaNO_3$ precipitation. The possible interactions between strontium, sodium and hydroxide are shown as equations (2) and (3).

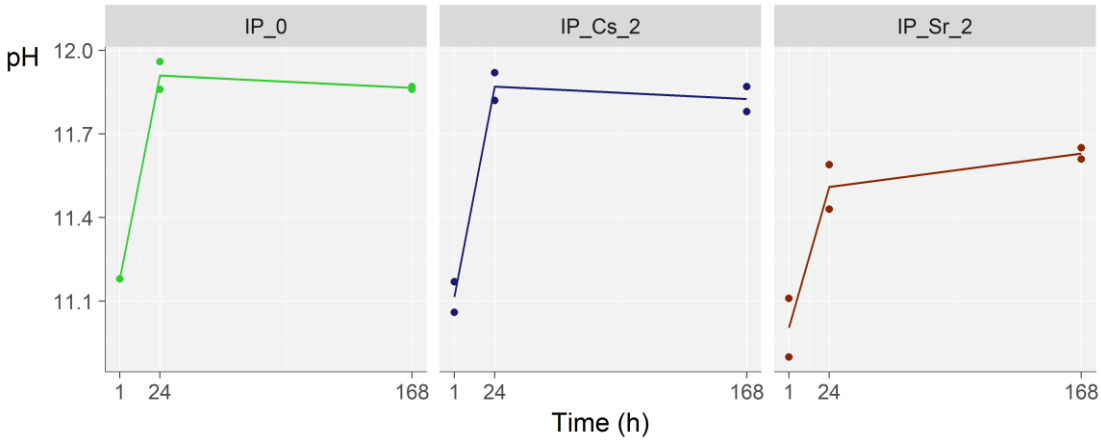

Figure 10: pH-values of eluates at different sampling times.

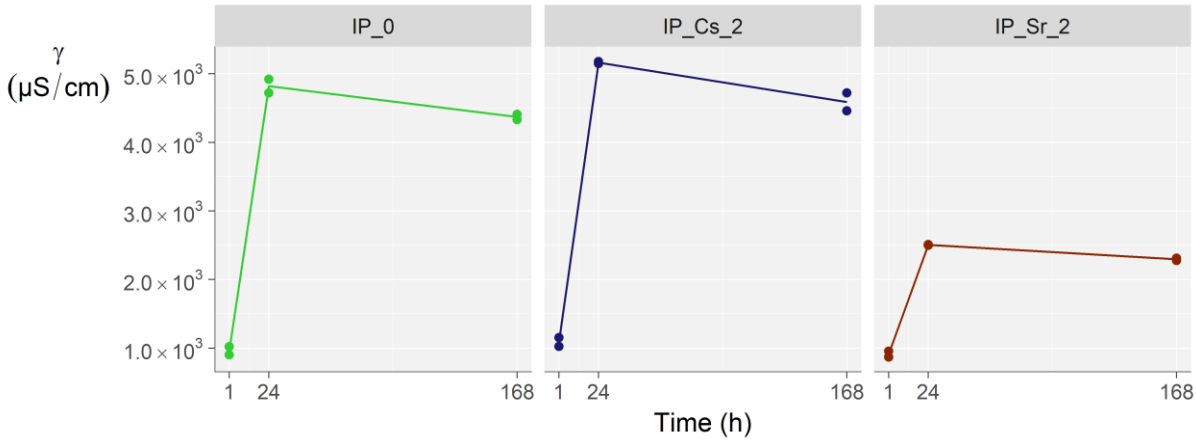

Figure 11: Conductivity γ (µS/cm) of eluates at different sampling times.

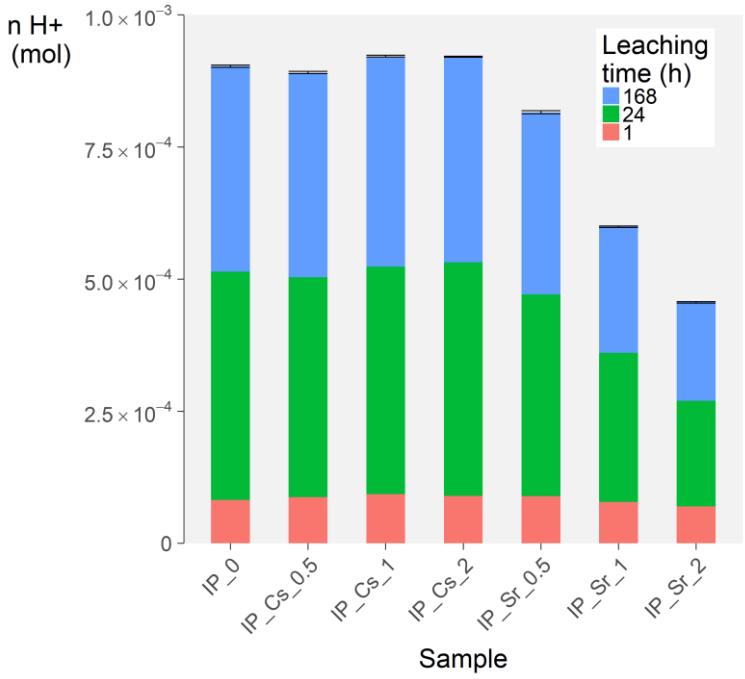

Figure 12: Cumulative amounts of H^+-ions added to neutralize the eluate (covering three equivalence points of pH ≈ 10, pH ≈ 8.5, and pH ≈ 5).

4 Conclusion

In this paper, the effect of adding Sr^{2+} and Cs^+ to a GGBFS-based IP was discussed. Sr^{2+} and Cs^+ were added, as nitrates, to a base IP-mixture to account for 0.5, 1, and 2 wt% of the final IP-mass. Calorimetric results indicate that Cs^+ did not show any significant effect on the early reaction kinetics. Sr^{2+}, however, severely affected the reaction kinetics by forming $Sr(OH)_2$ immediately after introducing the activating solution to the dry precursor. This consumed part of the available hydroxides resulting in a reduced dissolution of the precursor and thus a reduced polymerization reaction. This is also visible in the lower compressive and flexural strength. The micro-chemical analysis shows that almost all of the introduced Cs^+ is incorporated in the IP-matrix, while only about one-sixth of the introduced Sr^{2+} is incorporated into the matrix phase. It was also observed that adding caesium caused a decrease in the Ca^{2+}-content in the IP-matrix. Water absorption

experiments show that water absorption and apparent porosity of the samples is very low, and not significantly affected by the addition of caesium or strontium. From the leaching experiments, results show that Cs^+-leaching is proportional to the amount of Cs^+ added. For all caesium-containing samples, the final amount of Cs^+ released were all around 65 % of the introduced amount. The total Sr^{2+}-release was around 3 % of the introduced amount for each strontium-containing sample. Strontium-addition resulted in an increased Ca^{2+}-leaching while causing a significant decrease in the amount of Na^+ and OH^- leached. In general, the addition of Cs^+ did not show any significant effect on the studied parameters. Adding Sr^{2+}, however, caused an important decrease in the number of hydroxides available for the dissolution of the precursor resulting in a lower overall strength. For IP_Sr_0.5, the 1-day and 28-day compressive strength show no significant decrease compared to IP_0. Since the addition of 0.5 wt% Sr^{2+} results in a delayed setting time of 140 % in addition to the base sample[24][24][24][24], the application of strontium as a retarder in inorganic polymer development seems very promising. In future work, optimisation of the IP-composition for improved Cs^+ and Sr^{2+} immobilisation will be studied.

Acknowledgements

The authors would like to thank the research group of Applied and Analytical Chemistry (TANC) of Hasselt University for the ICP-OES and ICP-MS measurements. The authors would also like to thank the research group of Physical Chemistry and Polymer Science of the Vrije Universiteit Brussel (VUB), and in particular Prof. dr. ir. Hubert Rahier and ir. Antigoni Katsiki, for the calorimetric measurements.

References

[1] International Atomic Energy Agency, The behaviours of cementitious materials in long term storage and disposal of radioactive waste : results of a coordinated research project, Vienna, 2013.

[2] Q. Guangren, L. Yuxiang, Y. Facheng, S. Rongming, Improvement of metakaolin on radioactive

Sr and Cs immobilization of alkali-activated slag matrix, J. Hazard. Mater. 92 (2002) 289–300. doi:10.1016/S0304-3894(02)00022-5.

[3] M. Ochs, D. Mallants, L. Wang, Radionuclide and Metal Sorption on Cement and Concrete, Springer International Publishing, 2016. doi:10.1007/978-3-319-23651-3.

[4] C. Kuenzel, J.F. Cisneros, T.P. Neville, L. Vandeperre, S.J.R. Simons, J. Bensted, C.R. Cheeseman, Encapsulation of Cs/Sr contaminated clinoptilolite geopolymers produced from metakaolin, J. Nucl. Mater. 466 (2015) 94–99.

[5] S. Goni, A. Guerrero, M.P. Lorenzo, Efficiency of fly ash belite cement and zeolite matrices for immobilizing cesium, J. Hazard. Mater. 137 (2006) 1608–1617. doi:10.1016/j.jhazmat.2006.04.059.

[6] E. Wieland, J. Tits, D. Kunz, R. Dähn, Strontium Uptake By Cementitious Materials, Environ. Sci. Technol. 42 (2008) 403–409.

[7] J. Tits, E. Wieland, C.J. Müller, C. Landesman, M.H. Bradbury, Strontium binding by calcium silicate hydrates, J. Colloid Interface Sci. 300 (2006) 78–87. doi:10.1016/j.jcis.2006.03.043.

[8] M.Y. Khalil, E. Merz, Immobilization of intermediate-level wastes in geopolymers, J. Nucl. Mater. 211 (1994) 141–148. doi:10.1016/0022-3115(94)90364-6.

[9] G. Qian, D.D. Sun, J.H. Tay, New aluminium-rich alkali slag matrix with clay minerals for immobilizing simulated radioactive Sr and Cs waste, J. Nucl. Mater. 299 (2001) 199–204. doi:10.1016/S0022-3115(01)00700-0.

[10] A. Fernandez-Jimenez, D.E. MacPhee, E.E. Lachowski, A. Palomo, Immobilization of cesium in alkaline activated fly ash matrix, J. Nucl. Mater. 346 (2005) 185–193. doi:10.1016/j.jnucmat.2005.06.006.

[11] C. Shi, a. Fernández-Jiménez, Stabilization/solidification of hazardous and radioactive wastes with alkali-activated cements, J. Hazard. Mater. 137 (2006) 1656–1663. doi:10.1016/j.jhazmat.2006.05.008.

[12] M.G. Blackford, J. V. Hanna, K.J. Pike, E.R. Vance, D.S. Perera, Transmission electron microscopy and nuclear magnetic resonance studies of geopolymers for radioactive waste immobilization, J. Am. Ceram. Soc. 90 (2007) 1193–1199. doi:10.1111/j.1551-2916.2007.01532.x.

[13] Q. Li, Z. Sun, D. Tao, Y. Xu, P. Li, H. Cui, J. Zhai, Immobilization of simulated radionuclide 133Cs+ by fly ash-based geopolymer, J. Hazard. Mater. 262 (2013) 325–331. doi:10.1016/j.jhazmat.2013.08.049.

[14] J.G. Jang, S.M. Park, H.K. Lee, Physical barrier effect of geopolymeric waste form on diffusivity of cesium and strontium, J. Hazard. Mater. 318 (2016) 339–346. doi:10.1016/j.jhazmat.2016.07.003.

[15] J. Wang, J.X. Wang, Q. Zhang, Y.X. Li, Immobilization of simulated low and intermediate level waste in alkali-activated slag-fly ash-metakaolin hydroceramics, Nucl. Eng. Des. 300 (2016) 67–73. doi:10.1016/j.nucengdes.2016.01.011.

[16] Z. Li, T. Ohnuki, K. Ikeda, Development of Paper Sludge Ash-Based Geopolymer and Application to Treatment of Hazardous Water Contaminated with Radioisotopes, Materials (Basel). 9 (2016) 633. doi:10.3390/ma9080633.

[17] Z. Xu, Z. Jiang, D. Wu, X. Peng, Y. Xu, N. Li, Y. Qi, P. Li, Immobilization of strontium-loaded zeolite A by metakaolin based-geopolymer, Ceram. Int. 43 (2017) 4434–4439.

525 doi:10.1016/j.ceramint.2016.12.092.

526 [18] J.L. Provis, P.A. Walls, J.S.J. van Deventer, Geopolymerisation kinetics. 3. Effects of Cs and Sr
527 salts, Chem. Eng. Sci. 63 (2008) 4480–4489. doi:10.1016/j.ces.2008.06.008.

528 [19] X. Peng, Y. Xu, Z. Xu, D. Wu, D. Li, Effect of Simulated Radionuclide Strontium on
529 Geopolymerization Process, Procedia Environ. Sci. 31 (2016) 325–329.
530 doi:10.1016/j.proenv.2016.02.043.

531 [20] K. Komnitsas, D. Zaharaki, G. Bartzas, Effect of sulphate and nitrate anions on heavy metal
532 immobilisation in ferronickel slag geopolymers, Appl. Clay Sci. 73 (2013) 103–109.
533 doi:10.1016/j.clay.2012.09.018.

534 [21] K. Gong, C.E. White, Impact of chemical variability of ground granulated blast-furnace slag on
535 the phase formation in alkali-activated slag pastes, Cem. Concr. Res. 89 (2016) 310–319.
536 doi:10.1016/j.cemconres.2016.09.003.

537 [22] J. Jang, S. Park, H. Lee, Cesium and Strontium Retentions Governed by Aluminosilicate Gel in
538 Alkali-Activated Cements, Materials (Basel). 10 (2017). doi:10.3390/ma10040447.

539 [23] European Committee for Standardization, EN 196-6:2010 - Methods of testing cement - Part
540 6: Determination of fineness, 2010.

541 [24] N. Vandevenne, R.I. Iacobescu, Y. Pontikes, K. Gijbels, S. Schreurs, W. Schroeyers, THE EFFECT
542 OF Cs AND Sr ON THE MECHANICAL PROPERTIES OF BLAST FURNACE SLAG INORGANIC
543 POLYMER FOR RADIOACTIVE WASTE IMMOBILISATION, in: 5th Int. Slag Valoris. Symp., 2017:
544 pp. 401–404.

545 [25] ISO, International Standard ISO 10545-3:1995 - Determination of water absorption, apparent
546 porosity, apparent relative density and bulk density, 1997.

547 [26] ASTM, C 1220 - 98 Standard Test Method for Static Leaching of Monolithic Waste Forms for
548 Disposal of Radioactive Waste, (1998).

549 [27] European Committee for Standardization, CEN/TS 15863:2015: Characterisation of waste -
550 Leaching behaviour test for basic characterisation - Dynamic monolithic leaching test with
551 periodic leachant renewal, under fixed test conditions, 2015.

552 [28] E. Najafi Kani, A. Allahverdi, J.L. Provis, Calorimetric study of geopolymer binders based on
553 natural pozzolan, J. Therm. Anal. Calorim. (2016) 1–10. doi:10.1007/s10973-016-5850-7.

554 [29] J.G.S. van Jaarsveld, J.S.J. van Deventer, L. Lorenzen, Potential use of geopolymeric materials
555 to immobilize toxic metals: Part I. Theory and applications, Miner. Eng. 10 (1997) 659–669.
556 http://dx.doi.org/10.1016/S0892-6875(97)00046-0.

557